Grand canonical ensemble of the extended two-site Hubbard model via a nonextensive distribution

Felipe Américo Reyes Navarro[1,2*]
Email: farnape@gmail.com

Eusebio Castor Torres-Tapia[2]
Email: magnetumclub@gmail.com

Pedro Pacheco Peña[3]
Email: ppedroa@hotmail.com

[1]Facultad de Ciencias Naturales y Matemática, Universidad Nacional del Callao (UNAC) Av. Juan Pablo II 306, Bellavista, Callao, Peru

[2]Facultad de Ciencias Físicas, Universidad Nacional Mayor de San Marcos (UNMSM) Av. Venezuela s/n Cdra. 34, Apartado Postal 14-0149, Lima 14, Peru

[3]Universidad Nacional Tecnológica del Cono Sur (UNTECS), Av. Revolución s/n, Sector 3, Grupo 10, Mz. M Lt. 17, Villa El Salvador, Lima, Peru

[*]Corresponding author. Facultad de Ciencias Físicas, Universidad Nacional Mayor de San Marcos (UNMSM), Av. Venezuela s/n Cdra. 34, Apartado Postal 14-0149, Lima 14, Peru

Abstract

We hereby introduce a research about a grand canonical ensemble for the extended two-site Hubbard model, that is, we consider the intersite interaction term in addition to those of the simple Hubbard model. To calculate the thermodynamical parameters, we utilize the nonextensive statistical mechanics; specifically, we perform the simulations of magnetic internal energy, specific heat, susceptibility, and thermal mean value of the particle number operator. We found out that the addition of the intersite interaction term provokes a shifting in all the simulated curves. Furthermore, for some values of the on-site Coulombian potential, we realize that, near absolute zero, the consideration of a chemical potential varying with temperature causes a nonzero entropy.

Keywords

Extended Hubbard model, Quantum statistical mechanics, Thermal properties of small particles

PACS

75.10.Jm, 05.30.-d,65.80.+n

Introduction

Currently, several researches exist on the subject of the application of a generalized statistics for magnetic systems in the literature [1-3]. Specially, we are encouraged by the recent interesting results for small magnetic systems obtained in [4-6]. Nevertheless, herein, we will utilize a different system to that utilized in the previously cited references. Thus, the scope of our investigation is the computer simula-

tion on the one-dimensional extended Hubbard model for *M* dimers by considering a grand canonical ensemble. The tool we utilize to calculate several thermodynamical parameters is the nonextensive statistical mechanics; along with it, we use the Newton-Raphson method for numerical approximations. With regard to applications, we must mention that, in the scientific literature, the organic compound called tetracyanoquinodimethane has been studied as a dimer gas [7,8]; also, there are studies on a dimerized Hubbard chain [9,10]. We expect our results to contribute to the clarification of the possible use of nonextensive statistical mechanics to research low-dimensional systems. Also, as a particular case of our outcomes, we expect to confirm previous results from the simple Hubbard model.

The Hubbard model was proposed in the early 1960s by the British physicist John Hubbard [11-13]; basically, this model is the simplest one that takes into account the degrees of freedom linked to the electronic translational components. It has been applied to explain certain physical phenomena such as the metal-insulator transition, Mott insulators, ultracold atoms trapped in optical lattices, etc. [14,15]. On another side, in considering the several generalized statistical theories, the nonextensive statistical mechanics, also known as Tsallis statistics, is undoubtedly the most widely researched [16-20]. It was invented by the Brazilian professor C. Tsallis as a theory that generalizes the Boltzmann-Gibbs-Shannon statistics [21]. Although several versions of the Tsallis statistics exist, in this article we will deploy the third version that was proposed in 1998 [22]. All of those versions differ in the way of defining the thermal mean values.

This paper is structured as follows: the section 'Theoretical frame' contains the theoretical aspects, the subsection 'Two-site Hubbard model' tackles the two-site Hubbard model, and the subsection 'Nonextensive statistical mechanics' deals with the nonextensive statistical mechanics. The section 'Computer simulations' introduces the utilized numerical procedure as well as the results of the computer simulations carried out. In the section 'Conclusions,' we express the conclusions concerned with this investigation. Also, in the 'Acknowledgment', we thank the esteemed colleagues who provided useful information for this work.

Theoretical frame

In this section, we will display the fundamentals of the one-dimensional extended Hubbard model as well as the elementary features of the nonextensive statistical mechanics. We will study the Hubbard model in a Hilbert-Fock quantum space; also, we will show how to get the Tsallis distribution through the maximum entropy method.

Two-site Hubbard model

In a grand canonical ensemble, the one having a variable particle number, the Hamiltonian operator of the simple Hubbard model for a dimerized system is as follows:

$$\hat{H}_{\text{dimer}} = -t \sum_{\sigma} (c^{+}_{1,\sigma} c_{2,\sigma} + c^{+}_{2,\sigma} c_{1,\sigma}) + U \sum_{j} n_{j,\uparrow} n_{j,\downarrow} - h \sum_{j} (n_{j,\uparrow} - n_{j,\downarrow}), \tag{1}$$

where the indexes σ represent spins which may be up ($\uparrow$) or down ($\downarrow$), the indexes j designate sites 1 and 2 of the respective dimer, and t is the hopping integral for the kinetic energy term (the first one). Besides, in the framework of the second quantization, $c^{+}_{1,\sigma}$ is the creation operator that originates a particle with spin σ in site 1, and $c_{2,\sigma}$ symbolizes the annihilation operator that destructs a particle with spin σ in site 2. For the on-site interaction term (the second one), U stands for the Coulombian potential energy, $n_{1,\uparrow}$ represents the operator of particle number with spins $\uparrow$ in site 1, and $n_{1,\downarrow}$ symbolizes the operator of particle number with spins $\downarrow$ in site 1; all terms are similar for site 2. Lastly, in the third summand, h is

an external magnetic field.

To take into account the extended Hubbard model [23], we need to add another energy term to Equation 1, namely the intersite Coulombian interaction:

$$\hat{H}_{\text{intersite}} = J_1 \sum_{\sigma} n_{1,\sigma} n_{2,\sigma} \quad + \quad J_2 \sum_{\sigma} n_{1,\sigma} n_{2,-\sigma}, \tag{2}$$

with J_1 and J_2 denoting interactions between neighboring sites 1 and 2 inside each dimer; they are Coulombian repulsions modified by polaron effects. Consequently, we can group the two earlier equations to form the total Hamiltonian operator:

$$\hat{H}_{\text{dimer}} = -t \sum_{\sigma} (c^{+}_{1,\sigma} c_{2,\sigma} + c^{+}_{2,\sigma} c_{1,\sigma}) + U \sum_{j} n_{j,\uparrow} n_{j,\downarrow} + J_1 \sum_{\sigma} n_{1,\sigma} n_{2,\sigma} + J_2 \sum_{\sigma} n_{1,\sigma} n_{2,-\sigma} - h \sum_{j} (n_{j,\uparrow} - n_{j,\downarrow}). \tag{3}$$

Energy eigenvalues and eigenvectors in the two-site Hubbard model

To attain the energy eigenvalues, we have to build the Hamiltonian matrix; for that purpose, in the context of the Dirac algebra, we make use of the following basis of 16 vectors:

$$\begin{aligned} &|\ \Phi_1\ \rangle = |\ 0,\ 0\ \rangle,\ |\ \Phi_2\ \rangle = |\ \uparrow,\ 0\ \rangle,\ |\ \Phi_3\ \rangle = |\ \downarrow,\ 0\ \rangle,\ |\ \Phi_4\ \rangle = |\ 0, \uparrow\rangle,\ |\ \Phi_5\ \rangle = |\ 0, \downarrow\rangle,\ |\ \Phi_6\ \rangle = |\ \uparrow\downarrow,\ 0\rangle, \\ &|\ \Phi_7\ \rangle = |\ \uparrow, \uparrow\ \rangle,\ |\ \Phi_8\ \rangle = |\ \uparrow, \downarrow\ \rangle,\ |\ \Phi_9\ \rangle = |\ \downarrow, \uparrow\ \rangle, |\Phi_{10}\ \rangle = |\ \downarrow, \downarrow\rangle,\ |\Phi_{11}\rangle = |\ 0, \uparrow\downarrow\rangle,\ |\Phi_{12}\rangle = |\ \downarrow, \uparrow\downarrow\rangle, \\ &|\Phi_{13}\rangle = |\ \uparrow, \uparrow\downarrow\rangle,\ |\Phi_{14}\rangle = |\ \uparrow\downarrow, \downarrow\rangle,\ |\Phi_{15}\rangle = |\ \uparrow\downarrow, \uparrow\rangle,\ \text{and}\ \ |\Phi_{16}\rangle = |\ \uparrow\downarrow, \uparrow\downarrow\rangle. \end{aligned} \tag{4}$$

Inside each ket, the comma symbol separates site 1 from site 2, and the spins may be up or down. Then, each matrix element of $\hat{H}_{\text{dimer}}$ is obtained from the next bracketing operation:

$$[H_{\text{dimer}}]_{m,n} = \langle \Phi_m | \hat{H}_{\text{dimer}} | \Phi_n \rangle, \tag{5}$$

that is, to get each of the 256 matrix elements, we must consider two steps: (1) apply $\hat{H}_{\text{dimer}}$ on the respective ket and (2) apply the respective bra to the expression obtained from step 1. Making this, we have for step 1 (we lay down $\hat{H}_{\text{d}} \equiv \hat{H}_{\text{dimer}}$)

$$\begin{aligned} &\hat{H}_{\text{d}}|\Phi_1\rangle = 0,\ \hat{H}_{\text{d}}|\Phi_2\rangle = -t|\Phi_4\rangle - h|\Phi_2\rangle,\ \hat{H}_{\text{d}}|\Phi_3\rangle = -t|\Phi_5\rangle + h|\Phi_3\rangle,\ \hat{H}_{\text{d}}|\Phi_4\rangle = -t|\Phi_2\rangle - h|\Phi_4\rangle, \\ &\hat{H}_{\text{d}}|\Phi_5\rangle = -t|\Phi_3\rangle + h|\Phi_5\rangle,\ \hat{H}_{\text{d}}|\Phi_6\rangle = -t\big(|\Phi_9\rangle + |\Phi_8\rangle\big) + U|\Phi_6\rangle,\ \hat{H}_{\text{d}}|\Phi_7\rangle = (J_1 - 2h)|\Phi_7\rangle, \\ &\hat{H}_{\text{d}}|\Phi_8\rangle = -t\big(|\Phi_6\rangle + |\Phi_{11}\rangle\big) + J_2|\Phi_8\rangle,\ \hat{H}_{\text{d}}|\Phi_9\rangle = -t\big(|\Phi_6\rangle + \Phi_{11}\rangle\big) + J_2|\Phi_9\rangle, \\ &\hat{H}_{\text{d}}|\Phi_{10}\rangle = (J_1 + 2h)|\Phi_{10}\rangle,\ \hat{H}_{\text{d}}|\Phi_{11}\rangle = -t\big(|\Phi_8\rangle + |\Phi_9\rangle\big),\ \hat{H}_{\text{d}}|\Phi_{12}\rangle = -t|\Phi_{14}\rangle + x|\Phi_{12}\rangle, \\ &\hat{H}_{\text{d}}|\Phi_{13}\rangle = -t|\Phi_{15}\rangle + y|\Phi_{13}\rangle,\ \hat{H}_{\text{d}}|\Phi_{14}\rangle = -t|\Phi_{12}\rangle + x|\Phi_{14}\rangle,\ \hat{H}_{\text{d}}|\Phi_{15}\rangle = -t|\Phi_{13}\rangle + y|\Phi_{15}\rangle \\ &\text{and}\ \ \hat{H}_{\text{d}}|\Phi_{16}\rangle = 2(U + J_1 + J_2)|\Phi_{16}\rangle, \end{aligned} \tag{6}$$

where we set $x = U + J_1 + J_2 + h$ and $y = U + J_1 + J_2 - h$. By applying step 2, we achieve the 16×16 Hermitian matrix of Equation 3:

$$H_{\mathrm{d}} \doteq \begin{pmatrix}
0 & 0 & 0 & 0 & 0 & 0 & 0 & 0 & 0 & 0 & 0 & 0 & 0 & 0 & 0 & 0 \\
0 & -h & 0 & 0 & 0 & 0 & 0 & 0 & 0 & 0 & 0 & 0 & 0 & 0 & 0 & 0 \\
0 & 0 & h & 0 & 0 & 0 & 0 & 0 & 0 & 0 & 0 & 0 & 0 & 0 & 0 & 0 \\
0 & 0 & 0 & -h & 0 & 0 & 0 & 0 & 0 & 0 & 0 & 0 & 0 & 0 & 0 & 0 \\
0 & 0 & 0 & 0 & h & 0 & 0 & 0 & 0 & 0 & 0 & 0 & 0 & 0 & 0 & 0 \\
0 & 0 & 0 & 0 & 0 & U & 0 & -t & -t & 0 & 0 & 0 & 0 & 0 & 0 & 0 \\
0 & 0 & 0 & 0 & 0 & 0 & J_1 - 2h & 0 & 0 & 0 & 0 & 0 & 0 & 0 & 0 & 0 \\
0 & 0 & 0 & 0 & 0 & -t & 0 & J_2 & 0 & 0 & -t & 0 & 0 & 0 & 0 & 0 \\
0 & 0 & 0 & 0 & 0 & -t & 0 & 0 & J_2 & 0 & -t & 0 & 0 & 0 & 0 & 0 \\
0 & 0 & 0 & 0 & 0 & 0 & 0 & 0 & 0 & J_1 + 2h & 0 & 0 & 0 & 0 & 0 & 0 \\
0 & 0 & 0 & 0 & 0 & 0 & 0 & -t & -t & 0 & U & 0 & 0 & 0 & 0 & 0 \\
0 & 0 & 0 & 0 & 0 & 0 & 0 & 0 & 0 & 0 & 0 & x & 0 & -t & 0 & 0 \\
0 & 0 & 0 & 0 & 0 & 0 & 0 & 0 & 0 & 0 & 0 & 0 & y & 0 & -t & 0 \\
0 & 0 & 0 & 0 & 0 & 0 & 0 & 0 & 0 & 0 & 0 & -t & 0 & x & 0 & 0 \\
0 & 0 & 0 & 0 & 0 & 0 & 0 & 0 & 0 & 0 & 0 & 0 & -t & 0 & y & 0 \\
0 & 0 & 0 & 0 & 0 & 0 & 0 & 0 & 0 & 0 & 0 & 0 & 0 & 0 & 0 & 2(x+y)
\end{pmatrix} \tag{7}$$

where the symbol $\doteq$ means *represented by*. After diagonalizing this mathematical object, we accomplish the energy eigenvalues given by the following:

$$\begin{aligned}
&\varepsilon_1 = 0,\ \ \varepsilon_2 = -t + h,\ \ \varepsilon_3 = t + h,\ \ \varepsilon_4 = t - h,\ \ \varepsilon_5 = -t - h,\ \ \varepsilon_6 = J_2,\ \ \varepsilon_7 = U, \\
&\varepsilon_8 = C + \frac{U + J_2}{2},\ \ \varepsilon_9 = -C + \frac{U + J_2}{2},\ \varepsilon_{10} = J_1 - 2h,\ \varepsilon_{11} = J_1 + 2h,\ \varepsilon_{12} = t + U + J_1 + J_2, \\
&\varepsilon_{13} = -t + U + J_1 + J_2,\ \varepsilon_{14} = t + U + J_1 + J_2,\ \varepsilon_{15} = -t + U + J_1 + J_2,\ \text{ and }\ \varepsilon_{16} = 2(U + J_1 + J_2)
\end{aligned} \tag{8}$$

with

$$C = \sqrt{\left(\frac{U - J_2}{2}\right)^2 + 4t^2}. \tag{9}$$

Concerning the corresponding eigenvectors, they are the following:

$$\begin{aligned}
&|E_1\rangle = |\Phi_1\rangle,\ \ |E_2\rangle = \frac{1}{\sqrt{2}}\Big(|\Phi_2\rangle + |\Phi_4\rangle\Big),\ |E_3\rangle = \frac{1}{\sqrt{2}}\Big(|\Phi_2\rangle - |\Phi_4\rangle\Big), \\
&|E_4\rangle = \frac{1}{\sqrt{2}}\Big(|\Phi_3\rangle + |\Phi_5\rangle\Big),\ |E_5\rangle = \frac{1}{\sqrt{2}}\Big(|\Phi_3\rangle - |\Phi_5\rangle\Big),\ \ |E_6\rangle = \frac{1}{\sqrt{2}}\Big(|\Phi_8\rangle + |\Phi_9\rangle\Big), \\
&|E_7\rangle = \frac{1}{\sqrt{2}}\Big(|\Phi_6\rangle - |\Phi_{11}\rangle\Big),\ \ |E_8\rangle = a_1\Big(|\Phi_6\rangle + |\Phi_{11}\rangle\Big) - a_2\Big(|\Phi_8\rangle - |\Phi_9\rangle\Big), \\
&|E_9\rangle = a_2\Big(|\Phi_6\rangle + |\Phi_{11}\rangle\Big) + a_1\Big(|\Phi_8\rangle - |\Phi_9\rangle\Big),\ \ |E_{10}\rangle = |\Phi_7\rangle,\ |E_{11}\rangle = |\Phi_{10}\rangle, \\
&|E_{12}\rangle = \frac{1}{\sqrt{2}}\Big(|\Phi_{12}\rangle + |\Phi_{14}\rangle\Big),\ |E_{13}\rangle = \frac{1}{\sqrt{2}}\Big(|\Phi_{12}\rangle - |\Phi_{14}\rangle\Big),\ \ |E_{14}\rangle = \frac{1}{\sqrt{2}}\Big(|\Phi_{13}\rangle + |\Phi_{15}\rangle\Big), \\
&|E_{15}\rangle = \frac{1}{\sqrt{2}}\Big(|\Phi_{13}\rangle - |\Phi_{15}\rangle\Big),\ \ \text{and}\ \ |E_{16}\rangle = |\Phi_{16}\rangle;
\end{aligned} \tag{10}$$

the meanings of a_1 and a_2 are as follows:

$$a_1 = \frac{1}{2}\sqrt{1 + \frac{U - J_2}{2C}} \qquad \text{and} \qquad a_2 = \frac{1}{2}\sqrt{1 - \frac{U - J_2}{2C}}. \tag{11}$$

Finally, we take advantage of the energy eigenstates to affirm they are also eigenstates of the magnetic dipolar momentum operator $\hat{m}$; the respective *k*th eigenvalue of this last operator is as follows:

$$m_i = n_u - n_d \tag{12}$$

where n_u means the particle number with spins $\uparrow$ at the *k*th eigenstate, and n_d means the particle number with spins $\downarrow$ at the *k*th eigenstate. We want to emphasize these particle numbers are not evaluated at the states of Equation 4, but they are determinate from the states of Equation 10. Explicitly, the eigenvalues of $\hat{m}$ are the following:

$$\begin{array}{l} m_1 = 0,\ m_2 = m_3 = 1,\ m_4 = m_5 = -1,\ m_6 = m_7 = m_8 = m_9 = 0,\ m_{10} = 2, \\ m_{11} = -2,\ m_{12} = m_{13} = -1,\ m_{14} = m_{15} = 1,\ \text{ and }\ m_{16} = 0. \end{array} \tag{13}$$

Nonextensive statistical mechanics

The Tsallis entropy underlies this theory which was postulated in 1988 [21]. The entropic form is shown as follows:

$$S_q = k_{\mathrm{B}} \frac{1 - \sum\limits_i (p_i^q)}{q - 1}, \tag{14}$$

with p_i being the probability distribution to find the system in the *i*th state, p_i^q represents p_i powered to the entropic index q, k_{B} is the Boltzmann constant, and $\sum\limits_i (p_i^q)$ symbolizes the quantum operation of trace over all states of the matrix p_i^q. In Equation 14, the limit q tending to 1 allows us to recover the well-known Boltzmann-Gibbs-Shannon entropy:

$$S = -\ k_{\mathrm{B}} \sum_i \left[p_i \mathrm{Ln}(p_i) \right]. \tag{15}$$

The nonextensive probability distribution p_i is obtained by application of the maximum entropy method, a procedure formulated by the American Edward T. Jaynes [24,25]. In that method we consider these constraints for a grand canonical system:

$$\sum_i p_i = 1, \qquad E_q = \frac{\sum\limits_i p_i^q \epsilon_i}{\sum\limits_i p_i^q}, \quad \text{and} \quad N_q = \frac{\sum\limits_i p_i^q n_i}{\sum\limits_i p_i^q} \tag{16}$$

where E_q is the internal energy, ϵ_i denotes the energy eigenvalues of the energy operator $\hat{H}$, N_q is the quantum mean value of the particle number operator $\hat{N}$, and n_i is the eigenvalue of this last operator. As a final result of applying the maximum entropy method, we obtain the probability distribution

$$p_i = \frac{\left[1 - (1-q) \frac{\beta}{C_q} (\epsilon_i - E_q - \mu n_i + \mu N_q) \right]^{\frac{1}{1-q}}}{Z_q}, \tag{17}$$

Z_q being the partition function:

$$Z_q = \sum_i \left[1 - (1-q) \frac{\beta}{C_q} (\epsilon_i - E_q - \mu n_i + \mu N_q) \right]^{\frac{1}{1-q}}, \tag{18}$$

where $C_q = \sum\limits_i p_i^q$, β and μ are two out of the three Lagrange parameters - because of the three above constraints - utilized to optimize the Tsallis entropy, and the third parameter is one. Logically, we

recover the standard distribution for $q = 1$:

$$p_i = \frac{\exp\Big(-\beta(\epsilon_i - \mu n_i)\Big)}{\sum_j \exp\Big(-\beta(\epsilon_j - \mu n_j)\Big)}. \tag{19}$$

When we carry out the computer simulations, we will deploy the next definition of temperature T:

$$\frac{1}{k_{\rm B}T} = \frac{\beta}{C_q}; \tag{20}$$

however, we must mention that apart of this definition, in the literature, there are other ones because so far the matter regarding temperature is an open problem [26]. In addition, in Equations 17 and 18, it is mandatory to take into account the Tsallis cutoff (to guarantee the positivity of the probabilities):

$$\Delta = \left[1 - (1-q)\frac{1}{k_{\rm B}T}(\epsilon_i - E_q - \mu n_i + \mu N_q)\right] \geq 0. \tag{21}$$

Thereupon, the distribution of probability can be compacted as follows:

$$p_i = \begin{cases} \frac{\left[1 - (1-q)\frac{1}{k_{\rm B}T}(\epsilon_i - E_q - \mu n_i + \mu N_q)\right]^{\frac{1}{1-q}}}{Z_q}, & \text{if } \Delta \geq 0 \\ 0, & \text{otherwise.} \end{cases} \tag{22}$$

Thus, we can state a critical value of temperature $T_{\rm c}$. Above it, the *i*th probability is different from zero; below it, the *i*th probability is zero (but the other 15 probabilities which may be nonzero for $T \leq T_{\rm c}$ exist). Considering $k_{\rm B} = 1$, this decisive temperature is as follows:

$$T_{\rm c} = (1-q)(\epsilon_i - E_c - \mu n_i + \mu N_c) \tag{23}$$

where E_c and N_c are respectively E_q and N_q evaluated at $T = T_{\rm c}$. It is obvious that the last equation is a recursive formula. Thus, in the section 'Computer simulations,' we will use the Newton-Raphson method to calculate the thermal mean values.

On another side, the expressions for S_q and p_i can be rewritten utilizing the q-exponential and q-logarithmic functions

$$\mathrm{e}_q(x) = \left[1 + (1-q)x\right]^{\frac{1}{1-q}} \quad \text{and} \quad \mathrm{Ln}_q(x) = \frac{x^{1-q} - 1}{1-q}; \tag{24}$$

thus, the replacement of these expressions into S_q and p_i, Equations 14 and 17, gives the following:

$$\begin{aligned} p_i &= \frac{\mathrm{e}_q(-\frac{1}{k_{\rm B}T}[\epsilon_i - E_q - \mu n_i + \mu N_q])}{\sum_j \mathrm{e}_q(-\frac{1}{k_{\rm B}T}[\epsilon_j - E_q - \mu n_j + \mu N_q])} \qquad \text{and} \\ S_q &= -k\sum_i \left[p_i \mathrm{Ln}_q(p_i)\right] \end{aligned} \tag{25}$$

which, clearly, remember the entropy and the probability distribution for the Boltzmann-Gibbs-Shannon statistics.

The quantum mean values of any observable, represented by the operator $\hat{O}$, in the Hilbert-Fock space are calculated through the following formula:

$$O_q = \langle \hat{O} \rangle = \frac{\sum\limits_i p_i^q O_i}{\sum\limits_i p_i^q}, \tag{26}$$

where O_i stands for the *i*th eigenvalue of the observable $\hat{O}$. Naturally, the limit $q \to 1$ of the last expression becomes the known one

$$O = \langle \hat{O} \rangle = \sum_i p_i O_i. \tag{27}$$

Thus, using Equations 17, 18, and 26, we have the internal energy and mean value of the particle number operator which can be expressed explicitly as follows:

$$\begin{aligned} E_q &= \frac{\sum\limits_i \left[1-(1-q)\frac{1}{k_{\mathrm{B}}T}(\epsilon_i - E_q - \mu n_i + \mu N_q)\right]^{\frac{q}{1-q}} \varepsilon_i}{\sum\limits_j \left[1-(1-q)\frac{1}{k_{\mathrm{B}}T}(\epsilon_j - E_q - \mu n_j + \mu N_q)\right]^{\frac{q}{1-q}}} \quad \text{and} \\ N_q &= \frac{\sum\limits_i \left[1-(1-q)\frac{1}{k_{\mathrm{B}}T}(\epsilon_i - E_q - \mu n_i + \mu N_q)\right]^{\frac{q}{1-q}} n_i}{\sum\limits_j \left[1-(1-q)\frac{1}{k_{\mathrm{B}}T}(\epsilon_j - E_q - \mu n_j + \mu N_q)\right]^{\frac{q}{1-q}}}. \end{aligned} \tag{28}$$

Undeniably, these two thermodynamical parameters are defining two recurrence relations. These parameters will be found via Newton-Raphson method, as shown in the next section. Also, with respect to the magnetization, it is determined from the following formula:

$$M_q = \langle \hat{m} \rangle = \frac{\sum\limits_i p_i^q m_i}{\sum\limits_i p_i^q}, \tag{29}$$

where m_i stands for eigenvalues of the magnetic dipolar momentum operator $\hat{m}$. Additionally, other two thermodynamical parameters can be obtained if we derive the internal energy and magnetization, respectively. Thus, we obtain the specific heat

$$C_e = \frac{\partial E_q}{\partial T} \tag{30}$$

and the magnetic susceptibility

$$\chi = \left.\frac{\partial M_q}{\partial h}\right|_{h=0}. \tag{31}$$

Finalizing this section, we want to lay emphasis upon the fact that it is the chemical potential μ that controls the results for the grand canonical ensemble. Thus, we will utilize the following relation to that parameter:

$$\mu = \mu_0 + \alpha(T - T_0) \tag{32}$$

where μ_0 represents the initial chemical potential, α is a constant, T is the changing temperature, and T_0 is the initial temperature.

Computer simulations

In this section, we display the numerical procedure we utilized and the computer simulations obtained from it.

Numerical procedure

As mentioned before, the formulas of Equation 28 are recursive, and it will be necessary to apply the Newton-Raphson method to find E_q and N_q. In consequence, we have to form two functions in which E_q and N_q will be the respective roots. Therefore, we define $F_1(E_q,N_q) \equiv F_1 = 0$ with

$$F_1 = E_q - \frac{\sum_i \left[1-(1-q)\frac{1}{k_{\mathrm{BT}}}(\epsilon_i - E_q - \mu n_i + \mu N_q)\right]^{\frac{q}{1-q}} \epsilon_i}{\sum_i \left[1-(1-q)\frac{1}{k_{\mathrm{B}}T}(\epsilon_i - E_q - \mu n_i + \mu N_q)\right]^{\frac{q}{1-q}}}, \tag{33}$$

and $F_2(E_q,N_q) \equiv F_2 = 0$ with

$$F_2 = N_q - \frac{\sum_i \left[1-(1-q)\frac{1}{k_{\mathrm{B}}T}(\epsilon_i - E_q - \mu n_i + \mu N_q)\right]^{\frac{q}{1-q}} n_i}{\sum_i \left[1-(1-q)\frac{1}{k_{\mathrm{B}}T}(\epsilon_i - E_q - \mu n_i + \mu N_q)\right]^{\frac{q}{1-q}}}. \tag{34}$$

Furthermore, the earlier mentioned method provides us the following iterative relations:

$$E_{q,k+1} = E_{q,k} - \frac{F_{1,k}\frac{\partial F_{2,k}}{\partial N_q} - F_{2,k}\frac{\partial F_{1,k}}{\partial N_q}}{\frac{\partial F_{1,k}}{\partial E_q}\frac{\partial F_{2,k}}{\partial N_q} - \frac{\partial F_{1,k}}{\partial N_q}\frac{\partial F_{2,k}}{\partial E_q}} \tag{35}$$

and

$$N_{q,k+1} = N_{q,k} - \frac{F_{2,k}\frac{\partial F_{1,k}}{\partial E_q} - F_{1,k}\frac{\partial F_{2,k}}{\partial E_q}}{\frac{\partial F_{1,k}}{\partial E_q}\frac{\partial F_{2,k}}{\partial N_q} - \frac{\partial F_{1,k}}{\partial N_q}\frac{\partial F_{2,k}}{\partial E_q}}. \tag{36}$$

We will deploy as initial guesses those from the standard statistics, namely E_q and N_q with $q = 1$.

Magnetic thermodynamical parameters

We will display computer simulations of the following magnetic thermodynamical properties: entropy per dimer, internal energy per dimer, specific heat per dimer, susceptibility per dimer, and mean value per dimer of the particle number operator. Furthermore, in order to reduce the parameters involved in the simulations, we will assume the relation $J_1 = J_2 \equiv J$ for the intersite interaction term as well as $k_{\mathrm{B}} = 1$ for the Boltzmann constant. Even more, we define the normalized variables $T_t \equiv \frac{T}{t}$, $U_t \equiv \frac{U}{t}$, $J_t \equiv \frac{J}{t}$, and $h_t \equiv \frac{h}{t}$.

Figure 1 shows the entropy vs. the normalized temperature, i.e., S_q vs. T_t, with entropic index values $q = 1.0$, 1.2, 1.4, 1.7, and 2.0. On the left side of Figure 1, we do not consider the intersite interaction,

that is, $J_t = 0$; we have $U_t = 1$, 6, and 10, respectively, to Figure 1a,b,c. For these three graphics, we deploy $h_t = 0$ as well. In Figure 1a, at low temperature when $T \to 0$, $S_q \to 0$; the existence of a region where augmenting q means increasing S_q is apparent. However, at high temperature, we perceive that the landscape is completely opposite: augmenting q means decreasing S_q. With regard to Figure 1b,c, different nonzero values for entropy approaching to 0 exist; however, if we consider $\mu = \frac{U_t}{2}$ (independent of temperature), the entropy will be zero, as reported in [4]. On the right side of Figure 1, we take into account the intersite interaction term, that is, $U_t = 1$ and $J_t = 0.2$ in Figure 1d, $U_t = 6$ and $J_t = 3$ in Figure 1e, and $U_t = 10$ and $J_t = 5$ in Figure 1f; also, we lay down $h_t = 0$ to these three subfigures. In Figure 1d, it is evident that there is a small displacement towards the right side. However, this shift is enough notorious in Figure 1e,f. Likewise, in these last two graphics, we perceive that the entropy saturates so much before T_t borders on the absolute zero.

Figure 1 Entropy vs. normalized temperature. The values for q, U_t, J_t, and h_t are indicated inside each graphic. On the left side (**a** to **c**), we have no intersite interplay, but on the right side (**d** to **f**), we take into account it.

In Figure 2, we exhibit the normalized internal energy vs. the normalized temperature, E_q vs. T_t; the values of q are 1.0, 1.2, 1.4, 1.7, and 2.0. On the left side of Figure 2, we have no intersite interaction, $J_t = 0$. We take into account $U_t = 1$ in Figure 2a, $U_t = 6$ in Figure 2b, and $U_t = 10$ in Figure 2c; besides, we consider $h_t = 0$ in the three left subfigures. When contrasting Figure 2a from Figure 2b,c, we notice that the increase of U_t causes the expansion of the curves E_q. On the right side of Figure 2, we consider the interplay between neighboring sites for each dimer. Thus, we set $J_t = 0.2$, 3, and 5, respectively, to Figure 2d,e,f; the respective values of U_t and h_t are those from the left graphics. In Figure 2d, we realize the ground-state energy augments approximately to -1.4 (when it is contrasted with Figure 2a). However, in Figure 2e,f, we perceive the following: (1) the ground-state energy holds immutable when we add the intersite interaction term, and (2) in the low temperature range, the curves shift to the right side. However, at high temperatures, an increase of the values of E_q is visible.

Figure 2 Internal energy vs. normalized temperature. Inside each graphic, the respective values for q, U_t, J_t, and h_t are shown. Side by side (**a** to **f**), we have internal energy with and without intersite interaction.

Figure 3 displays graphs of the specific heat vs. the normalized temperature, C vs. T_t, with entropic index $q = 1.0$, 1.2, 1.4, 1.7, and 2.0. In Figure 3a, we have $U_t = 1$, in Figure 3b we set $U_t = 6$, and in Figure 3c, we lay down $U_t = 10$. For all three earlier cases, $J_t = 0$ and $h_t = 0$. In Figure 3a, we have only a peak due to the antiparallel order; we perceive three regions verifying only one of the following statements: (1) the greater q, the lesser C, and (2) the greater q, the greater C. In Figure 3b,c, we have two peaks: the first one is due to the antiparallel order, and the second one is provoked by the metal-insulator transition. In Figure 3b, three regions similar to those from Figure 3a are evident; however, between $T_t \approx 0.7$ and $T_t \approx 1.7$, the existence of a region that does not verify the above statements 1 and 2 is visible. In Figure 3c, four regions verifying either statement 1 or 2 exist. On another side, in contrast with the left side graphics, the right side graphics set the intersite interaction. Thus, we have $J_t = 0.2$, 3, and 5, respectively, in Figure 3d,e,f. In Figure 3d, an almost imperceptible movement of the curves towards the right side has happened. However, that displacement is more than noticeable so in Figure 3e as well as in Figure 3f. The intersite interaction causes the destruction of the second peak appearing in Figure 3b, as seen in Figure 3e. Notwithstanding, in Figure 3f, for $q = 1$, the peak due to antiparallel order maintains yet; for $q \neq 1$, that first peak does not exist anymore.

Figure 3 Specific heat vs. normalized temperature. The values for q, U_t, J_t, and h_t are shown inside each graphic. The left side graphics (**a** to **c**) have no intersite interplay, but the right side graphics (**d** to **f**) present it.

Figure 4 brings forward the magnetic susceptibility vs. the normalized temperature, χ *vs.* T_t, for $q =$ 1.0, 1.2, 1.4, 1.7, and 2.0. In Figure 4a,b,c, we calculate χ by using respectively $U_t = 1$, $U_t = 6$, and $U_t = 10$; furthermore, we consider $J_t = 0$ and $h_t = 0$ for all three cases. In these curves without intersite interaction, we also find three regions verifying only one of the following affirmations: (1) the greater q, the greater χ, and (2) the greater q, the lesser χ. Also, it is apparent that augmenting U_t means increasing the value of χ, a signal that the system is more localized. On another side, when we take into account the intersite interaction term $J_t = 0.2$ in Figure 4d, we detect a slight diminution of χ; however, the three regions from Figure 4a still exist. Nonetheless, augmenting the values of J_t provokes drastic drops for χ, as displayed in Figure 4e,f. Furthermore, we noticed that the addition of the intersite term caused the displacement of the curves towards the right side.

Figure 4 Magnetic susceptibility vs. normalized temperature. The values for q, U_t, J_t, and h_t are indicated inside each graphic. On the left side (**a** to **c**), we have no intersite interplay. However, on the right side (**d** to **f**), we have that interaction.

Lastly, in Figure 5, the thermal mean value of the particle number operator vs. the normalized temperature, i.e., N_q vs. T_t, with $q = 1.0$, 1.2, 1.4, 1.7, and 2.0, is presented. On the left side of Figure 5, we have $U_t = 1$, 6, and 10, respectively, in Figure 5a,b,c. For all of them, $J_t = 0$ and $h_t = 0$. In Figure 5a, we noticed that when T_t is zero, N_q saturates at 2; in increasing T_t, N_q drops but it augments again and tends towards 2 in high temperatures. The case of Figure 5b,c is completely different: around $T_t = 0$, N_q saturates at 1, and it never decreases. On the right side of Figure 5, we consider the intersite interaction. In Figure 5d, we see that this term causes N_q to lower slightly its value as T_t approaches 0.5. However, in Figure 5e,f, it was detected that the intersite interaction originates a drop that does not exist neither in Figure 5b nor in Figure 5c.

Figure 5 Mean value of particle number operator vs. normalized temperature. Inside each graphic, the respective values for q, U_t, J_t, and h_t are indicated. On the left side (**a** to **c**), we have no intersite interplay, though on the right side (**d** to **f**), we have that interaction.

Conclusions

In this article, we have introduced a research to calculate thermodynamical properties from a grand canonical ensemble of the extended two-site Hubbard model. The Tsallis statistics was utilized instead of the standard one because it would be more adequate to study low-dimensional systems for it exists several investigations in that regard. As concluding remarks, we can affirm that we have verified early results for the simple two-site Hubbard model. Also, we have found out that the addition of the intersite interaction term to the simple Hubbard model provoked a displacement of the curves of entropy, internal energy, specific heat, susceptibility, and mean value of the particle number operator, respectively; additionally, we have perceived that, near absolute zero, the consideration of a chemical potential varying with temperature causes a remnant of entropy, but it happens only at some values of the on-site Coulombian potential. A way of understanding the displacement of the curves is realizing the critical temperature changes because the Tsallis cutoff is satisfied with new conditions, i.e., the intersite interaction term determines new values for critical temperatures.

Competing interests

The authors declare that they have no competing interests.

Authors' contributions

FARN carried out the outline of the paper as well as proposed the main formulas. ECTT participated by providing additional formulas. PPP participated in critiquing and correcting the original draft. All authors read and approved the final manuscript.

Authors' information

FARN is a Peruvian and a doctor in physical sciences at the Brazilian Center for Physics Research (CBPF) located in Rio de Janeiro, Brazil. ECTT is a Peruvian and a doctor in physics at the *Universidade Federal do Rio de Janeiro* (UFRJ) located in Rio de Janeiro, Brazil. PPP is a Peruvian and a licentiate in physics at the *Universidad Nacional Mayor de San Marcos* (UNMSM) located in Lima, Peru.

Acknowledgment

We are very thankful to Professor M. Matlak - from the University of Silesia, Poland - for giving us updated references to elaborate this paper.

References

1. Reis MS, Araujo JP, Amaral VS, Lenzi EK, Oliveira IS (2002) Magnetic behavior of a nonextensive S-spin system: possible connections to manganites. Phys Rev B 66:134417
2. Reis MS, Amaral VS, Araujo JP, Oliveira IS (2003) Magnetic phase diagram for a nonextensive system: experimental connection with manganites. Phys Rev B 68:014404
3. Reis MS, Freitas JCC, Orlando MTD, Lenzi EK, Oliveira IS (2002) Evidences for Tsallis non-extensivity on CMR manganites. Europhysics Lett 58(1):42–48
4. Hasegawa H (2005) Nonextensive thermodynamics of the two-site Hubbard model. Physica A 351(2–4):273–293
5. Hasegawa H (2011) Thermal entanglement of Hubbard dimers in the nonextensive statistics. Physica A 390(8):1486–1503
6. Navarro FAR, Flores JFV (2011) Computer simulations for the extended Hubbard model utilizing nonextensive statistical mechanics. Revista de Investigación de Física de la UNMSM, Lima, Peru 14:111401755
7. Fowler M, Puga MW (1978) Dimer gas model for tetracyanoquinodimethane (TCNQ). Phys Rev B 18:421–428
8. Silverman BD (1981) Slipped versus eclipsed stacking of tetrathiafulvalene (TTF) and tetracyanoquinodimethane (TCNQ) dimers. Top Curr Phys: Crystal Cohesion Conformational Energies 26:108–136
9. Guo-Hui D, Fei Y, Bo-Wei X (2000) Charge and spin gaps in the dimerized Hubbard model. Chinese Phys 9:615–619

10. Bernstein U, Pincus P (1974) Thermodynamic properties of the dimerized half-filled-band Hubbard chain. Phys Rev B 10:3626–3634

11. Hubbard J (1963) Electron correlations in narrow energy bands. Proc. Royal Soc. of London. Ser A, Math Phys Sci 276(1365):238–257

12. Tasaki H (1998) The Hubbard model - an introduction and selected rigorous results. J Phys: Condensed Matt 10(20):4353–4378

13. Essler FHL, Frahm H, Göhmann F, Klümper A, Korepin VE (2005) The One-Dimensional Hubbard Model. Cambridge University Press, Cambridge

14. Jiang L (2009) Phase Transition in Strongly Correlated Systems: Bilayer Quantum Hall Effect, Inhomogeneous Superconductivity and Boson Hubbard Model. VDM Verlag, Saarbrücken

15. Macêdo MA, Macêdo CA (1999) Termodinâmica do modelo de Hubbard de dois átomos. Revista Brasileira de Ensino de Física 21(3):321–327

16. Tsallis C, Tirnakli U (2010) Nonadditive entropy and nonextensive statistical mechanics - some central concepts and recent applications. J Phys: Conf Ser 201:012001

17. Tsallis C (2004) What should a statistical mechanics satisfy to reflect nature? Physica D 193:3–34

18. Tsallis C (2009) Introduction to nonextensive statistical mechanics: Approaching a complex world. Springer, New York

19. Tsallis C (2012) Nonextensive statistical mechanics and thermodynamics. http://tsallis.cat.cbpf.br/biblio.htm. Accessed 7 March 2013

20. Ferri GL, Martinez S, Plastino A (2005) Equivalence of the four versions of Tsallis's statistics. J Stat Mech 193:P04009. [ArXiv:cond-mat/0503441]

21. Tsallis C (1988) Possible generalization of Boltzmann-Gibbs statistics. J Stat Phys 52(1–2):479–487

22. Tsallis C, Mendes RS, Plastino R (1998) The role of constraints within generalized nonextensive statistics. Physica A 261(3–4):534–554

23. Matlak M, Grabiec B, Krawiec S (2008) Fermionic lattice models and electronic correlations: magnetism and superconductivity. J. Non-Crystalline Solids 354(35–39):4326–4329. [ArXiv:cond-mat/0511329v1]

24. Jaynes ET (1957) Information theory and statistical mechanics. Phys Rev 106(4):620–630

25. Uhlenbeck G, Rosenzweig N, Siegert AJF, Jaynes ET, Fujita S (1963) Statistical physics. In: Brandeis University Summer Institute Lectures in Theoretical Physics 3. W.A. Benjamin, New York

26. Abe S, Martinez S, Pennini F, Plastino A (2001) Nonextensive thermodynamic relations. Phys Lett A 281(2–3):126–130

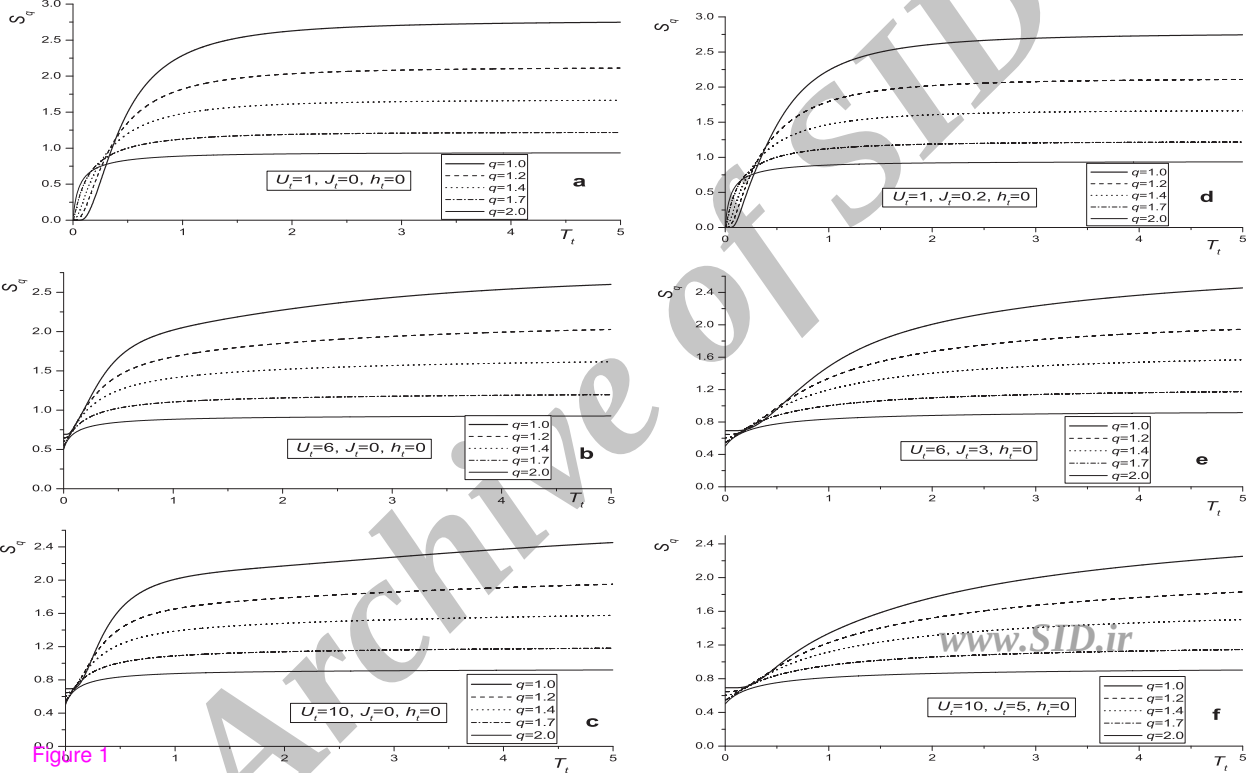

Figure 1

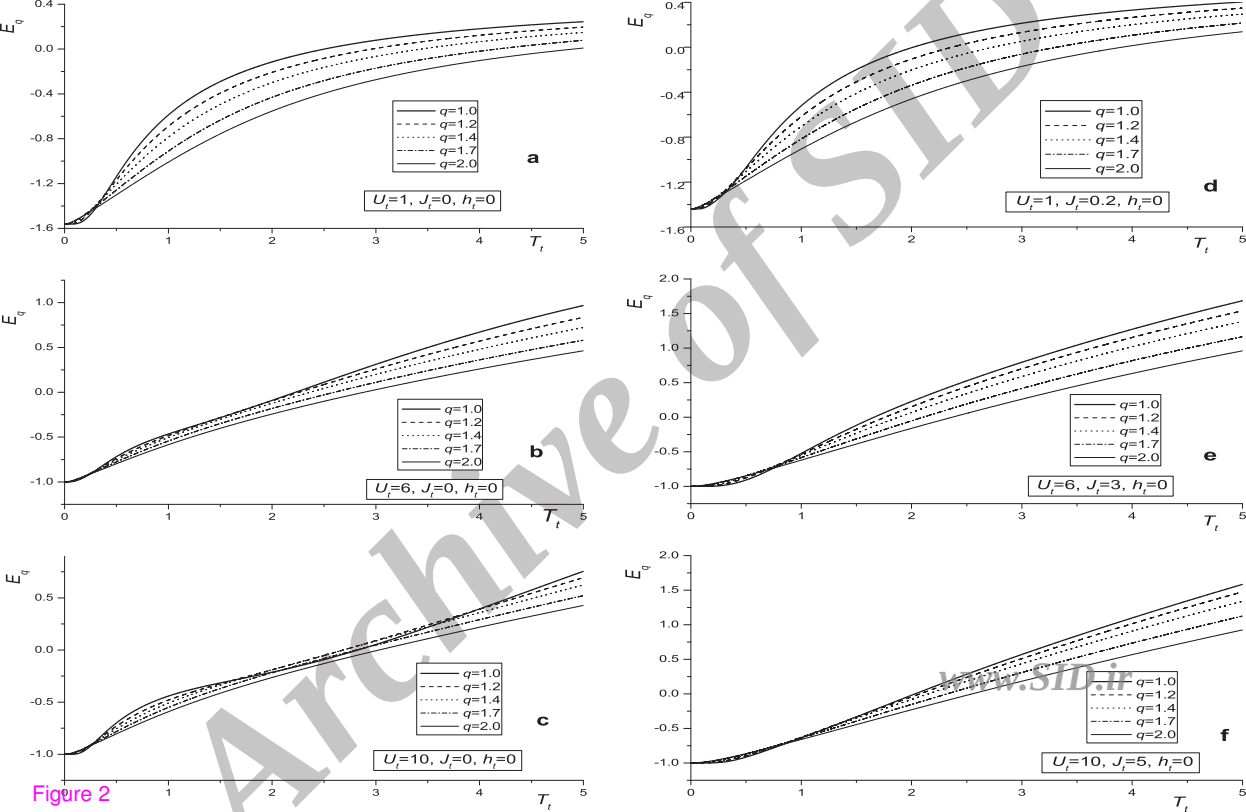

Figure 2

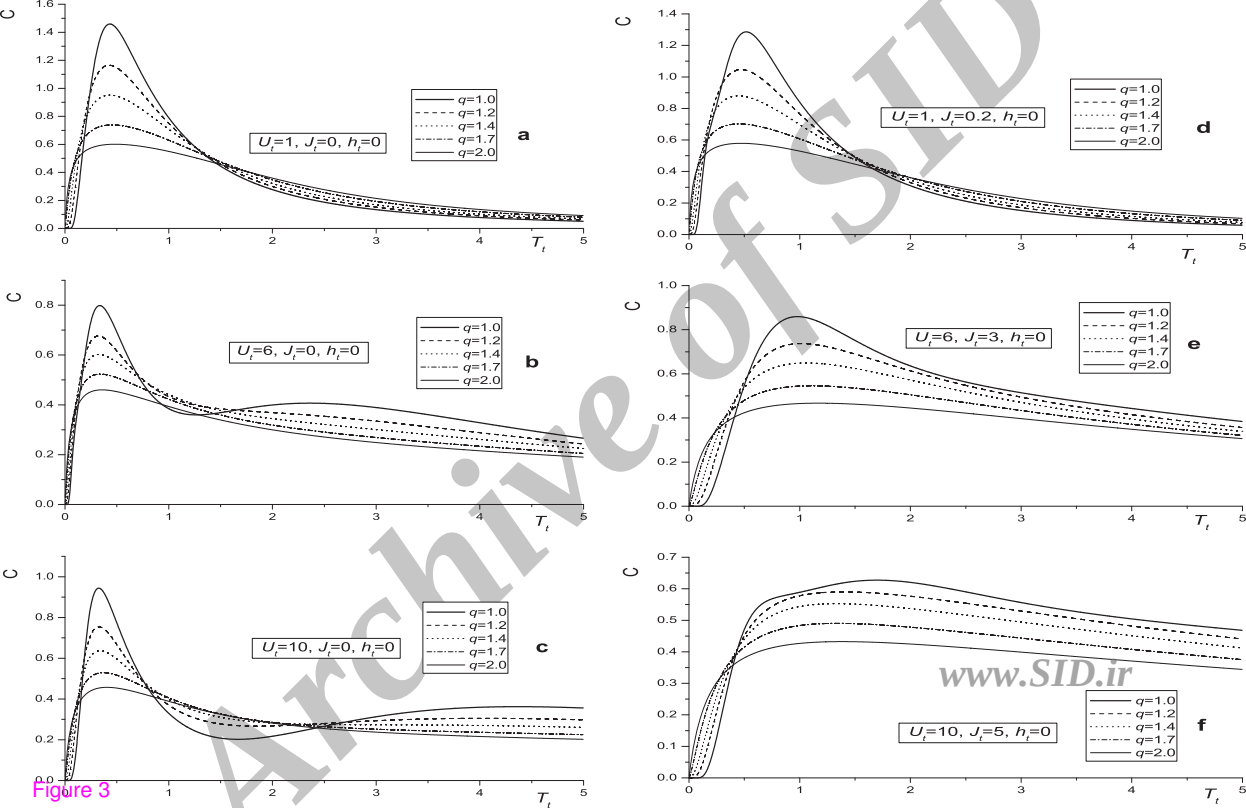

Figure 3

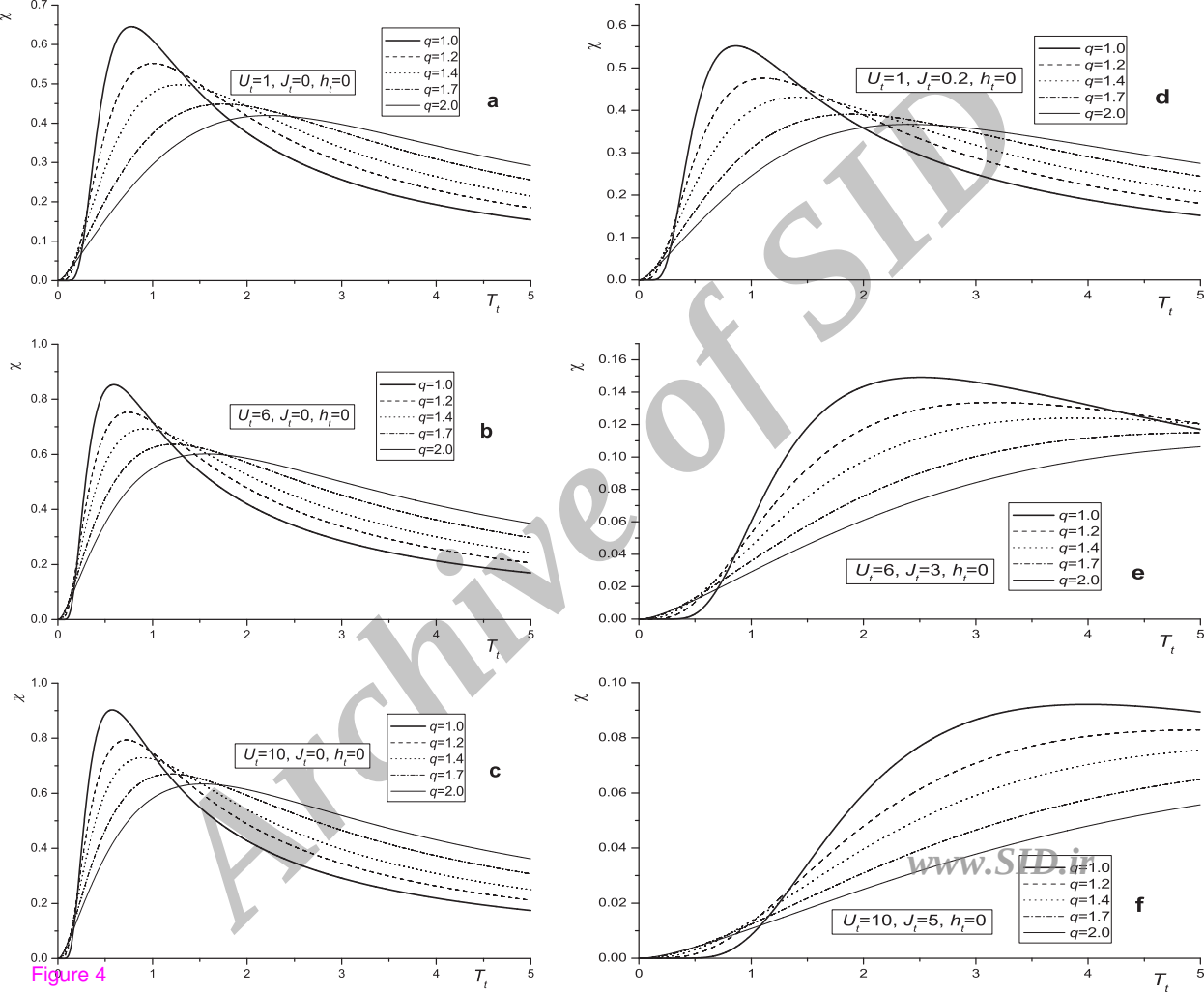

Figure 4

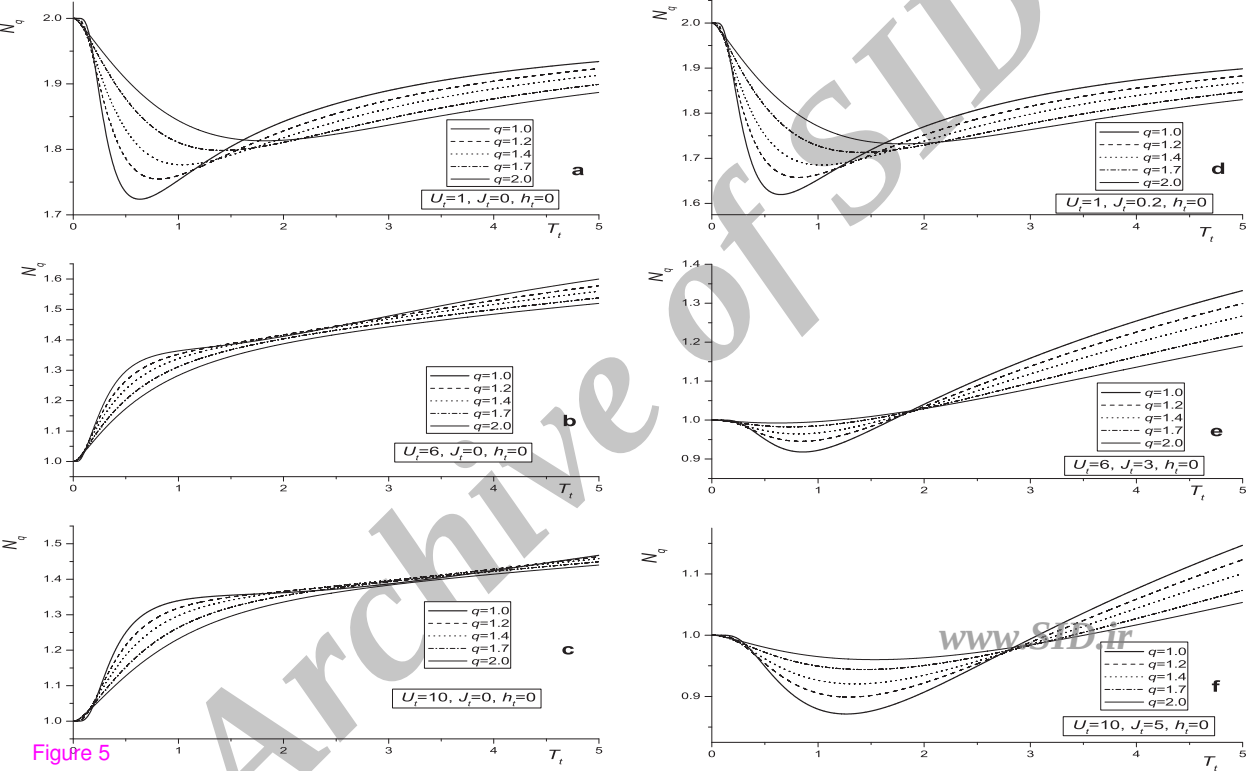

Figure 5

Additional files provided with this submission:

Additional file 1: Figure1PDF.PDF, 2623K
http://www.jtaphys.com/imedia/1606958960881123/supp1.pdf
Additional file 2: Figure2PDF.PDF, 2688K
http://www.jtaphys.com/imedia/4071007908811266/supp2.pdf
Additional file 3: Figure3PDF.PDF, 2689K
http://www.jtaphys.com/imedia/1523747561881133/supp3.pdf
Additional file 4: Figure4PDF.PDF, 2946K
http://www.jtaphys.com/imedia/2124597238881139/supp4.pdf
Additional file 5: Figure5PDF.pdf, 58K
http://www.jtaphys.com/imedia/3893506038811425/supp5.pdf
Additional file 6: 1143205554876622--corrected.tex, 38K
http://www.jtaphys.com/imedia/2979414219383662/supp6.tex
Additional file 7: BiblioHu.bib, 7K
http://www.jtaphys.com/imedia/1997459919938367/supp7.bib